




# Test of the gravitational redshift with single-photon-based atomic clock interferometers

Ju Liu<sup>1</sup>, Yaoyao Xu<sup>1\*</sup> , Huaqing Luo<sup>1</sup>, Lushuai Cao<sup>1</sup>, Minkang Zhou<sup>1</sup>, Xiaochun Duan<sup>1</sup> and Zhongkun Hu<sup>1\*</sup>

## Abstract

The gravitational redshift (GR), as predicted by Einstein's general theory of relativity, posits that two identical clocks situated at different gravitational potentials will tick at different rates. In this study, we explore the impact of the GR on a single-photon-based atom interferometer and propose a corresponding testing scheme. Our approach conceptualizes the atom interferometer as two coherent atomic clocks positioned at distinct elevations, which is referred to as an atomic clock interferometer, allowing us to derive the GR-induced phase shift. This effect becomes significant due to the notable energy difference between the two atomic internal states, comparable to other relativistic effects in single-photon-based atomic clock interferometers. Furthermore, our proposed scheme incorporates the velocity of the laser device to effectively mitigate other relativistic effects. The ensuing analysis indicates an anticipated GR test precision at the  $10^{-5}$  level for our proposed approach.

**Keywords:** Gravitational redshift, Atomic clock interferometer, Single-photon-based interferometer, Atom interferometer, General relativity

## 1 Introduction

The equivalence principle is the cornerstone of Einstein's theory of general relativity and has been consistent with every experimental test [1–5]. Despite its success in elucidating gravitational interactions, a notable challenge arises in the majority of theoretical models aiming to unify gravitation with the other three fundamental interactions, as they often necessitate a departure from the equivalence principle [6–8]. The gravitational redshift (GR), predicted by general relativity, stands out as a significant phenomenon predicting that a clock positioned at a higher gravitational potential will tick at a faster rate than an identical clock at a lower potential. To experimentally verify

this central prediction, various tests have been conducted utilizing advancements in the precision of atomic clocks. Recent experiments have taken advantage of space missions, comparing terrestrial atomic clocks with those in orbit [5, 9], and ground-based tests have also been performed, involving atomic clocks placed separately at the top and bottom of a tower [10]. These experiments have consistently yielded constraints on the GR test at a level of  $10^{-5}$ . Furthermore, noteworthy contributions to the GR test involve frequency gradient measurements across atomic ensembles at millimeter or centimeter scales within an optical lattice [11, 12]. All these experiments contribute valuable insights into the understanding and verification of the GR effect.

Atom interferometers play a pivotal role in discussions concerning the test of Einstein's equivalence principle [2, 4, 13–18]. Merged as significant tools for both inertial sensing and fundamental physics research [19–22], atom interferometers are employed not only for precision appli-

\*Correspondence: [xuyaoyaoleo@hust.edu.cn](mailto:xuyaoyaoleo@hust.edu.cn); [zkhu@hust.edu.cn](mailto:zkhu@hust.edu.cn)

<sup>1</sup>MOE Key Laboratory of Fundamental Quantities Measurement, Hubei Key Laboratory of Gravitation and Quantum Physics, School of Physics, Huazhong University of Science and Technology, Wuhan, 430074, People's Republic of China

cations in gravimetry [23–27] but also in tests of the universality of free fall (UFF) [13, 15–17] and local Lorentz invariance (LLI) [4, 14], other two basic assumptions of Einstein’s equivalence principle. While UFF and LLI have been scrutinized with remarkable precision, the GR test has encountered limitations in achieving comparable accuracy. GR, causing time dilation, manifests in the interference phase shift of an atom interferometer that compares phases accumulated along two spatially separated paths. This phase shift serves as an indicator of the proper time differences between the two branches. Expectations of GR effects in atom interferometers have prompted the development of specialized schemes [28–30]. Recent proposals utilize the recoil velocity of photons to introduce a centimeter-scale height difference in gravitational potential between the two branches. Despite these advancements, the precision of the GR test in atom interferometer remains at a relatively modest level, estimated at around  $10^{-3}$  [30]. The primary challenge lies in the energetic proximity of internal states involved in the interference process, resulting in a weak phase difference imprinted by the GR effect. Overcoming this limitation is crucial for further advancements in precision testing with atom interferometry.

Given the imperative to enhance atom interferometer measurement schemes for the GR test, our work focuses on analyzing GR-related phase through a perturbation method shifts in a single-photon-based Mach-Zehnder atom interferometer and presents a scheme for the GR test. The geometry of a Mach-Zehnder atom interferometer can be conceptualized as two sequential coherent atomic clocks operating at the frequency of the atomic internal state. Hence, we term this configuration an atomic clock interferometer (ACI) in this paper. The clocks in an ACI are positioned at different heights due to the free-fall of atoms in a gravitational field, leading to a GR-induced phase shift. To further enhance the precision of the GR test for ACIs, we propose the use of a drop tower to obtain a larger scale of height difference and a free-fall laser device to suppress disturbance effects. The paper is structured as follows: Sect. 2 provides a brief introduction to the Hamiltonian of the atomic system, presenting interference phases for both two-photon-based and single-photon-based ACIs. In Sect. 3, the corresponding interpretations of interference phases are expounded, and a scheme for the GR test utilizing a single-photon-based ACI is discussed in detail, followed by a conclusion in Sect. 4.

## 2 GR-induced phase shifts in ACIs

An ACI can be conceptualized as two sequential coherent atomic clocks operating at the frequency of the atomic internal state and positioned at different heights, as illustrated in Fig. 1(a). The ACI measures the phase difference accumulated along two distinct spatial paths, wherein

the GR introduces a contribution to this phase difference by influencing the ticking rates of internal atomic clocks based on the spatial path. To undertake a quantitative analysis of the interference phase shift, we delve into the Hamiltonian of the atomic system, considering low-order relativistic corrections. The energy of the atom is calculated as  $E = \sqrt{M^2c^4 + P^2c^2}$ , where

$$M = m + \frac{E_i}{c^2} \quad (1)$$

represents the total rest mass of an atom. According to the mass-energy equivalence, *the total rest mass contains an equivalent mass of internal energy  $E_i$* . The Hamiltonian under the laboratory reference frame can be expressed as [31]

$$\begin{aligned} H &= Mc^2 + \frac{P^2}{2M} + Mgz \\ &\approx \left( mc^2 + \frac{P^2}{2m} + mgz \right) + E_i \left( 1 - \frac{P^2}{2m^2c^2} + \frac{gz}{c^2} \right) \end{aligned} \quad (2)$$

The first term in Eq. (2) indicates the external state of atoms accelerating uniformly in a gravitational field, while the second term represents the relativistic correction of the atomic internal state. Especially for the second term,  $\frac{gz}{c^2}$  is the modification of the GR, and  $-\frac{P^2}{2m^2c^2}$  is the correction of the special relativity time dilation of internal dynamics. Treating the atomic internal state as a clock, the Hamiltonian of internal dynamics [32] can be written as  $H_i = E_i \left( 1 - \frac{P^2}{2m^2c^2} + \frac{gz}{c^2} \right) \approx E_i \frac{d\tau}{dt}$ , where  $\frac{d\tau}{dt}$  is the time-lapse coefficient of probe-time relative to coordinate-time.

### 2.1 Phase shift in two-photon-based ACIs

In a typical two-photon-based ACI, as outlined in Ref. [23], the interaction between atoms and lasers is based on a three-level system that encompasses two hyperfine ground states with energies  $E_e$  and  $E_g$ , as illustrated in Fig. 1(b). The ideal time intervals between laser-atom interactions are denoted as exactly equal to  $T$ . However, accounting for the finite speed of light (FSL), these intervals are not precisely  $T$  (depicted in Fig. 2(a)). Consequently, photons interact with atoms in different paths at different moments, introducing an additional difference in the free evolution of the atomic wave packet in each path and resulting in an additional spatial separation at the exit of the interference. Moreover, the time delay associated with the FSL can influence the laser phase at the moment of interaction, introducing an additional phase shift transmitted from the lasers. Accordingly, the interference phase shift is calculated by dividing it into three parts: phase  $\Delta\varphi_{\text{free}}$  is correlated with the free evolution of atomic wave packets along the classical paths, phase  $\Delta\varphi_{\text{laser}}$  is induced through the atom-laser interaction, and phase  $\Delta\varphi_{\text{separate}}$  arises from

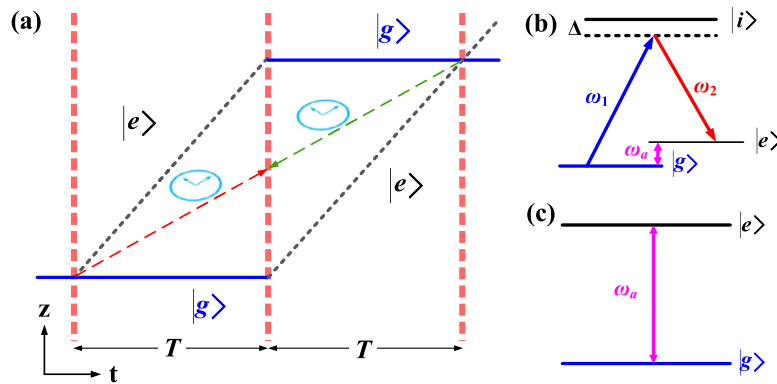


**Figure 1** Treat the atomic internal state as a ticking clock. (a) The ACI functions as if two coherent atomic clocks are ticking at the frequency of the atomic internal energy level. These clocks are positioned at different heights, giving rise to interference phase shifts attributable to the GR. The ticking frequency of the clocks is related to the energy level of the atom. The energy level diagrams for (b) two-photon-based and (c) single-photon-based ACIs. In the process of atom interference in (b), an atom initially in the ground state  $|g\rangle$  interacts sequentially with two photons and eventually reaches another ground state  $|e\rangle$ . The energy level difference between these two ground states is at the GHz level, equivalent to the frequency difference between the two lasers employed in the process. Conversely, in a single-photon-based ACI in (c), the atomic transition between two ground states  $|g\rangle$  and  $|e\rangle$  involves the absorption of just one photon. The energy level difference between the two ground states, precisely matching the laser frequency, is typically several hundreds of THz.

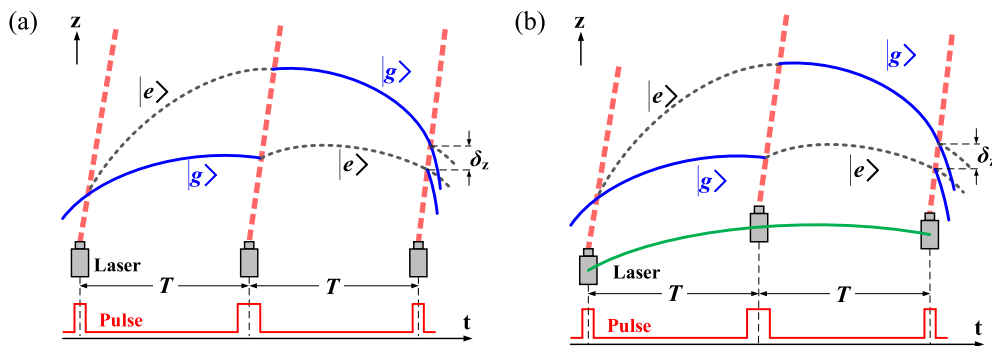


**Figure 2** Space-time diagrams of ACIs. Atoms undergo interactions with three laser pulses to achieve interference. (a) represents the case of the FSL. The blue and grey dashes represent the atoms at different internal states, while the red dash represents the motions of the photons. (b) is the space-time diagram while introducing a non-zero acceleration of the laser device. The motion of the laser device is illustrated by the green solid line

path separation at the exit of interference. This comprehensive breakdown allows for a detailed understanding and precise calculation of the interference phase shift in the ACI. The total interference phase shift can be written as  $\Delta\varphi_{\text{total}} = \Delta\varphi_{\text{free}} + \Delta\varphi_{\text{separate}} + \Delta\varphi_{\text{laser}}$ .

$\Delta\varphi_{\text{free}}$  is calculated by path integral method [33]. According to the Hamiltonian in Eq. (2), we obtain the Lagrangian as

$$L \approx -mc^2 - E_i + \frac{mv^2}{2} \left( 1 + \frac{E_i}{mc^2} \right) - \left( m + \frac{E_i}{c^2} \right) gz \quad (3)$$

$$\equiv L_0 + L_1$$

where the internal-state-related Lagrangian  $L_1 = -E_i \frac{dt}{dt} \approx -E_i \left( 1 - \frac{v^2}{2c^2} + \frac{gz}{c^2} \right)$  is considered as a perturbation of the external-state-related Lagrangian  $L_0 = -mc^2 + \frac{mv^2}{2} - mgz$ . Accordingly,  $\Delta\varphi_{\text{free}}$  can be calculated by

$$\Delta\varphi_{\text{free}} \approx -\frac{1}{\hbar} \int_{L_0} (L_0 + L_1) dt = \Delta\varphi_{\text{free}}^{\text{external}} + \Delta\varphi_{\text{free}}^{\text{internal}} \quad (4)$$

Here, the free evolution phases associated with external and internal states are denoted as  $\Delta\varphi_{\text{free}}^{\text{external}}$  and  $\Delta\varphi_{\text{free}}^{\text{internal}}$ , respectively. To simplify the calculation, we combine the free evolution phase shift related to the atomic external state  $\Delta\varphi_{\text{free}}^{\text{external}}$  with the phase shift introduced by the path separation  $\Delta\varphi_{\text{separate}}$ . For the closed loop of interference

path formed by the combination of the free evolution of atomic external states and the path separation in the gravitational field [34–37], we have

$$\Delta\varphi_{\text{free}}^{\text{external}} + \Delta\varphi_{\text{separate}} = \frac{mc^2}{\hbar} \oint \left( 1 - \frac{v^2}{2c^2} + \frac{gz}{c^2} \right) dt \quad (5)$$

$$\approx 0$$

Correspondingly, phase shift caused by the internal state during the free evolution is calculated as follows

$$\Delta\varphi_{\text{free}}^{\text{internal}} = \frac{1}{\hbar} \int_{L_0} E_i \left( 1 - \frac{v^2}{2c^2} + \frac{gz}{c^2} \right) dt \quad (6)$$

$$= k_a g T^2 + \frac{v_T}{c} k_a g T^2$$

Here,  $k_a = \omega_a/c$  represents the wave vector corresponding to the frequency difference  $\omega_a$  between the atomic hyperfine ground states, and  $v_T = v_0 + v_r - gT$  is the average velocity of atoms in both paths at the moment of applying the  $\pi$  pulse with  $v_r$  the recoil velocity and  $v_0$  the atomic velocity at the beginning of the interference.

The first-order relativistic effect of the internal state in Eq. (6) is further subdivided according to the following derivations. As displayed in Fig. 1(a), the ACI is divided into two coherent clocks at different heights, and the induced phase is expressed as  $\Delta\varphi = -[\int_{\text{up}} \omega_a \frac{gz}{c^2} dt - \int_{\text{low}} \omega_a \frac{gz}{c^2} dt]$ , which leads to a phase shift relating to the GR as

$$\Delta\varphi_{\text{redshift}} \approx -\frac{v_T}{c} k_a g T^2 \quad (7)$$

For phase shift induced by the special relativistic time dilation, a perturbation calculation  $\Delta\varphi_{\text{dilation}} = -\int_{L_0} E_i \frac{v^2}{2c^2} dt$  is adopted to obtain the phase shift of this effect as

$$\Delta\varphi_{\text{dilation}} \approx -\frac{v_T}{c} k_a g T^2 \quad (8)$$

The remaining phase shift of the first-order relativistic effect in  $\Delta\varphi_{\text{free}}^{\text{internal}}$  is  $\Delta\varphi_E = \frac{3v_T}{c} k_a g T^2$ , which represents the phase shift of the FSL effect of atomic internal states.

$\Delta\varphi_{\text{laser}}$  comes from the phase transmission from lasers to atoms during laser-atom interaction.  $\Delta\varphi_{\text{laser}}$  is calculated as

$$\Delta\varphi_{\text{laser}} = -\left[ \sum_i \pm\phi(x_i, t_i)|_{\text{up}} - \sum_i \pm\phi(x_i, t_i)|_{\text{low}} \right] \quad (9)$$

where  $\phi(x_i, t_i)$  represents the phase of lasers at the position  $x_i$  and the moment  $t_i$ , and the signs of + or – correspond to the atom gaining or losing momentum as a result of the interaction. Employing the average-path method [38], we denote the moments of interactions for the second and third

laser pulses during the interference as  $T_1 = T + \delta T_1$  and  $T_2 = 2T + \delta T_2$ , respectively, where

$$\begin{cases} \delta T_1 \approx \frac{(v_0 T + \frac{\hbar k T}{2m} - \frac{gT^2}{2})}{c} + \frac{(v_0 + \frac{\hbar k}{2m} - gT)(v_0 T + \frac{\hbar k T}{2m} - \frac{gT^2}{2})}{c^2} \\ \delta T_2 \approx \frac{(2v_0 T + \frac{\hbar k T}{m} - 2gT^2)}{c} + \frac{(v_0 + \frac{\hbar k}{2m} - 2gT)(2v_0 T + \frac{\hbar k T}{m} - 2gT^2)}{c^2} \end{cases} \quad (10)$$

As the two lasers propagate in opposite directions, they induce a phase expressed by

$$\Delta\varphi_{\text{laser}} = -2k_2 c \cdot (\delta T_2 - 2\delta T_1) \quad (11)$$

$$\approx 2k_2 g T^2 + \frac{3v_T}{c} 2k_2 g T^2$$

where  $k_2$  is the wave vector of the laser reflected by a mirror. However, compensating for the Doppler shift in experiments requires applying a frequency chirp to the lasers. Considering frequency chirping rates of  $-\alpha_1$  and  $\alpha_2$  for two lasers, the additional interference phase shift caused by frequency chirp is

$$\Delta\varphi_{\text{chirp}} \approx -\alpha_1 T^2 + \frac{\alpha_2}{2} [(2T + 2\delta T_2)^2 - 2(T + 2\delta T_1)^2] \quad (12)$$

$$\approx -(\alpha_1 - \alpha_2) T^2 + 2\alpha_2 \frac{(2v_0 + 2v_r - 3gT)}{c} T^2$$

Therefore, the total FSL effect phase from the lasers in a two-photon-based ACI can be expressed as  $[\frac{3v_T}{c} 2k_2 g + 2\alpha_2 \frac{(2v_0 + 2v_r - 3gT)}{c}] T^2$ , which includes the frequency chirp item. Based on the above calculations, the total phase shift is concluded as

$$\Delta\varphi_{\text{total}} \approx [2k_2 g - (\alpha_1 - \alpha_2)] T^2 \quad (13)$$

$$+ \left[ \frac{3v_T}{c} 2k_2 g + 2\alpha_2 \frac{(2v_0 + 2v_r - 3gT)}{c} \right] T^2$$

$$+ k_a g T^2 + \frac{v_T}{c} k_a g T^2$$

## 2.2 Phase shift in single-photon-based ACIs

A single-photon-based ACI usually employs the transition between two atomic internal states with a resonant frequency of hundreds of THz, resulting in a much larger  $k_a$  than that in a two-photon-based ACI (shown in Fig. 1(c)) [26, 39]. This distinction in energy level differences presents a key advantage of single-photon-based ACIs. The larger energy separation provides a more pronounced and easily detectable phase shift, enhancing the GR test accuracy of the interferometer. Referring to the above phase-shift calculation, the phase shift induced through the atom-laser interaction is written as

$$\Delta\varphi_{\text{laser}} = -\alpha_1 T^2 \quad (14)$$

**Table 1** A list of all the phase shift terms calculated above for both two-photon-based and single-photon-based ACIs, as well as for single-photon-based ACI in microgravity

|   | Two-photon-based ACI  | Single-photon-based ACIs | Single-photon-based ACIs in microgravity | Interpretation               |
|---|---|--------------------------|--|------------------------------|
| 1 | $2k_2gT^2 - (\alpha_1 - \alpha_2)T^2$                           | $-\alpha_1T^2$           | 0  | Laser frequency              |
| 2 | $k_agT^2$   | $k_agT^2$                | 0  | Internal state               |
| 3 | $[\frac{3v_T}{c}2k_2g + 2\alpha_2\frac{(2v_0+2v_T-3gT)}{c}]T^2$ | 0                        | 0  | FSL effect of lasers         |
| 4 | $-\frac{v_T}{c}k_agT^2$   | $-\frac{v_T}{c}k_agT^2$  | $-\frac{v_T}{c}k_agT^2$                  | GR                           |
| 5 | $-\frac{v_T}{c}k_agT^2$   | $-\frac{v_T}{c}k_agT^2$  | $-\frac{v_T}{c}k_agT^2$                  | Time dilation                |
| 6 | $\frac{3v_T}{c}k_agT^2$   | $\frac{3v_T}{c}k_agT^2$  | 0  | FSL effect of internal state |

Here, the phase item correlated with the FSL effect of lasers is eliminated due to the absence of  $k_2$ . The internal-state-induced part of the free evolution phase shift is calculated as  $\Delta\varphi_{\text{free}}^{\text{internal}} = k_agT^2 + \frac{v_T}{c}k_agT^2$  similar to Eq. (6), and the phase shifts induced by the GR and the special relativistic time dilation are  $\Delta\varphi_{\text{redshift}} = \Delta\varphi_{\text{dilation}} \approx -\frac{v_T}{c}k_agT^2$ , identical with the above calculations for the two-photon-based ACI. Generally, a single-photon-based ACI is applied to our model to calculate the total phase shift as

$$\Delta\varphi_{\text{total}} \approx (k_ag - \alpha_1)T^2 + \frac{v_T}{c}k_agT^2 \quad (15)$$

### 3 Scheme for the GR test

We propose a novel measurement scheme designed to detect the GR effect. In our setup, we employ a single-photon-based ACI, conducting measurements in a microgravity environment within the free-fall facility of a drop tower. Notably, the laser device responsible for generating the manipulation lasers is fixed within the free-fall chamber, falling simultaneously with the atoms in the experimental setup. This scheme offers significant advancements. Firstly, the GR-induced phase shift is amplified by utilizing a single-photon-based ACI because of the larger energy separation between the two ground states. Secondly, potential phase shifts induced by other sources like the FSL effect are effectively mitigated through the execution of the experiment in a microgravity environment within a drop tower. This approach enhances the precision of the measurement, providing a platform for studying the GR effect.

In a single-photon-based ACI, the GR effect is remarkably amplified. Despite the expresses for both single-photon-based and two-photon-based ACIs being summarized as  $\Delta\varphi_{\text{redshift}} \approx -\frac{v_T}{c}k_agT^2$  in Table 1, the energy difference between the two internal states experienced by an atom during the interference in a single-photon-based ACI is typically 5 orders of magnitude larger than that in a two-photon-based ACI [34]. Displayed in Fig. 3 with typical parameters are the main phase shifts for both types of ACIs. In two-photon-based ACIs, the GR effect is negligible compared to the comparatively small  $k_a$  of the hyperfine structures. Conversely, in single-photon-based ACIs

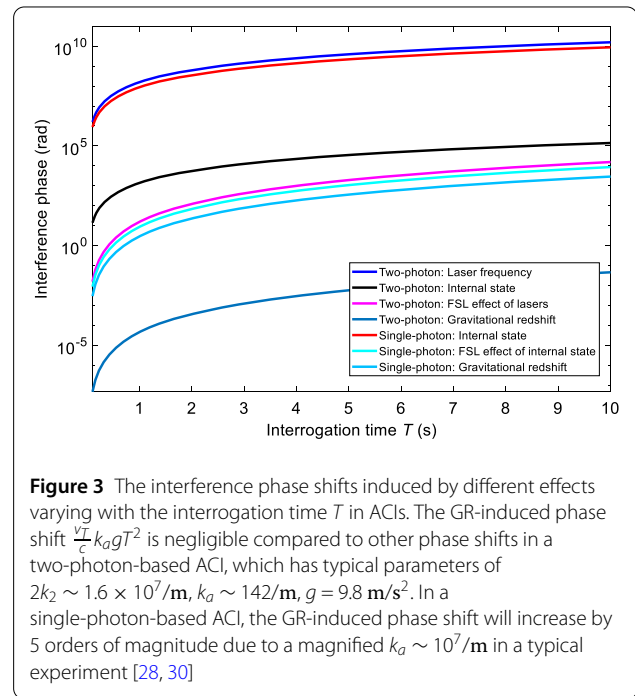


**Figure 3** The interference phase shifts induced by different effects varying with the interrogation time  $T$  in ACIs. The GR-induced phase shift  $-\frac{v_T}{c}k_agT^2$  is negligible compared to other phase shifts in a two-photon-based ACI, which has typical parameters of  $2k_2 \sim 1.6 \times 10^7/\text{m}$ ,  $k_a \sim 142/\text{m}$ ,  $g = 9.8 \text{ m/s}^2$ . In a single-photon-based ACI, the GR-induced phase shift will increase by 5 orders of magnitude due to a magnified  $k_a \sim 10^7/\text{m}$  in a typical experiment [28, 30]

in our calculation, the phase shift induced by the atom-laser interaction is calculated to be  $-\alpha_1T^2$  and the phase shift arising from the FSL effect of lasers equals zero because of the absence of  $k_2$  and  $\alpha_2$ . This results in a GR effect comparable to the FSL effect of the internal state. However, it's noteworthy that the non-relativistic phase shift term of  $(k_ag - \alpha_1)T^2$ , induced by atom-laser interaction and the evolution of internal states, still domains in a single-photon-based ACI and requires further suppressed.

The primary competing terms to the GR-induced phase shift come from the non-relativistic phase shift item and the FSL effect of the internal state. In our proposed scheme, we analyze how these disturbance terms are suppressed. In the preceding discussion, the laser device responsible for generating laser is fixed, while the atoms experience free fall in the Earth's gravitational. This implies that, in the Earth reference frame, both the initial velocity  $v_{\text{laser}}$  and the acceleration  $a$  of the laser device during the inter-



ference are zero. Considering the initial velocity  $v_{\text{laser}}$  and a uniform non-zero acceleration  $a$  of the laser device (as shown in Fig. 2(b)), the moments of interactions for the second and third laser pulses during the interference become  $T_1 = T + \delta T_1 + \delta T'_1$  and  $T_2 = 2T + \delta T_2 + \delta T'_2$ , respectively. Substituting  $T_1$  and  $T_2$  into the calculations above, we have the phase shifts as follows

$$\begin{cases} \Delta\varphi_{\text{laser}} = -\alpha_1 T^2 + \frac{3(v' - g'T)}{c} k_a g' T^2 \\ \Delta\varphi_{\text{free}} = k_a g' T^2 - \frac{2v_T}{c} k_a g' T^2 \\ \quad - \left( \frac{v_{\text{atom}}}{c} a - \frac{v_{\text{laser}}}{c} g \right) k_a T^2 \end{cases} \quad (16)$$

where  $v' = v_{\text{atom}} - v_{\text{laser}}$  is the difference between the initial velocities of the atom and laser device at the beginning of the interference, and  $g' = g - a$  denotes the acceleration difference. This consideration introduces a nuanced perspective on the temporal aspects of the laser-atom interactions during the interference process. Here, the phase shifts arising from the GR and the special relativistic time dilation remain identical to those in the situation of zero acceleration of the laser device. However, according to Eq. (16), the FSL effect phase shift  $\frac{3(v' - g'T)}{c} k_a g' T^2$  is variant with the velocity and acceleration of the laser device. By contrast, the phase shifts arising from GR, as well as special relativistic time dilation, remain independent of the motion of the laser device. These shifts are exclusively related to the internal states experienced by atoms during the interference. Generally, the total phase shift in a single-photon-based ACI with a moving laser device is calculated as

$$\begin{aligned} \Delta\varphi_{\text{total}} \approx & (k_a g' - \alpha_1) T^2 + \frac{3(v' - g'T)}{c} k_a g' T^2 \\ & - \frac{2v_T}{c} k_a g' T^2 - \left( \frac{v_{\text{atom}}}{c} a - \frac{v_{\text{laser}}}{c} g \right) k_a T^2 \end{aligned} \quad (17)$$

Microgravity is anticipated to play a pivotal role in advancing tests of the equivalence principle [40]. In our proposed scheme, we envision a single-photon-based ACI performing measurements in microgravity within the free fall facility of a drop tower. In this setup, a laser device is securely fixed within the free-fall chamber, descending simultaneously with the atoms. This configuration establishes relationships where the velocity of the atoms  $v_{\text{atom}}$  equals the velocity of the laser device  $v_{\text{laser}}$ , and the gravitational acceleration  $g$  is equivalent to the acceleration  $a$  experienced by the laser device. Additionally, due to the consistent relative velocity between the laser and atoms throughout the interference, the frequency chirp of the laser becomes unnecessary. This unique approach simplifies the experimental conditions and enhances the precision of the GR test in the microgravity environment of a drop tower. Introducing a GR violation factor  $\alpha$ , the effect of GR on internal atomic clocks in the Hamiltonian

of Eq. (2) is rewritten as  $(1 + \alpha)\frac{gz}{c^2}$ . Consequently, we have the total phase shift deduced from Eq. (17) as

$$\Delta\varphi_{\text{total}} \approx -\frac{(2 + \alpha)v_T}{c} k_a g T^2 \quad (18)$$

Equation (18) reveals that, under microgravity conditions, single-photon-based ACIs are affected solely by the GR and special relativistic time dilation, with the non-relativistic phase shift and phase shifts induced by the FSL effect being eliminated. The equivalent altitude difference relies on the coherent clocks in free-fall is  $\Delta z = v_T T$ . Considering typical parameters of  $v_T = 7$  m/s,  $k_a = 10^7$ /m, and  $T = 0.7$  s in a 10-meter drop tower, a GR test signal over 1 rad is obtained, corresponding to a relative test accuracy at the level of  $10^{-5}$  corresponding to an equivalent altitude difference of two coherent atomic clocks is 4.9 meters.

#### 4 Discussions and conclusions

The test of the GR effect necessitates information regarding the frequency difference between clocks situated at different heights. The GR test, when based on atomic clocks, can improve precision by augmenting the height difference between the two clocks. Although ACIs cannot achieve height differences comparable to those in atomic clock tests, the theoretical accuracy for the GR test in our proposed scheme is not inferior to experimental tests based on atomic clocks. This is primarily attributed to the distinct requirements these two approaches have for the precision of clock frequency measurements. In the GR tests based on atomic clocks, the initial step involves measuring the clock frequencies at different heights, and subsequently, the comparison of frequency differences between these clocks yields the corresponding signal for the GR test. This measurement process demands extremely high precision in clock frequency to achieve a meticulous test of the GR effect. On the contrary, ACIs can directly capture the phase information of the frequency difference accumulated over time due to the GR effect on clocks at different heights, which implying that the precision requirements for measuring clock frequencies using atomic interferometers are not particularly high. Furthermore, in our proposed scheme, we utilize the two atomic clocks arranged temporally in the ACI to test the GR effect. As atoms freely fall in a gravitational field, the clocks naturally assume different heights. In comparison to schemes [28, 30, 40] that involve the height difference induced by the momentum imparted by the absorbed photons, the height difference in our scheme can be increased by two orders of magnitude. This results in a corresponding two-order-of-magnitude enhancement in the GR test. The preceding discussion highlights the benefits of our GR test scheme and the considerable potential of single-photon-based ACIs. However, in comparison to two-photon-based ACIs, the construction of single-photon-based ACIs may necessitate more

intricate experimental conditions. On one hand, for single-photon-based ACIs employing Sr atoms, the upper-level linewidth of Sr atoms is only on the order of mHz. This requires the laser involved in atomic interactions to achieve higher intensity for a substantial Rabi frequency. On the other hand, unlike two-photon-based ACIs that are sensitive to the phase difference between two lasers, controllable through methods like phase-locked loops, single-photon-based ACIs are more susceptible to laser phase noise. Consequently, the employed lasers must attain better phase noise control. Nevertheless, the internal clock with a substantial frequency inherent in single-photon-based ACIs presents a potential demonstrating significant promise for GR tests. Research groups are actively advancing experimental studies on single-photon-based ACIs [41–45], with the prospect of their application in fields such as low-frequency gravitational wave detection [46, 47].

In summary, our calculations involve determining the first-order relativistic effects in both single-photon-based and two-photon-based ACIs, employing the Hamiltonian rooted in mass-energy equivalence. By treating a Mach-Zehnder atom interferometer as two coherent atomic clocks, we focused on the calculation of the GR effect. Our findings suggest that the GR effect in a single-photon-based ACI is significantly magnified, rendering it comparable to the FSL effect. To further enhance accuracy, we considered the motion of the laser device in the Earth reference frame. Introducing the velocity of the laser device proves advantageous in suppressing phase shifts induced by non-GR terms, including the non-relativistic effect and the FSL effect. Proposing the implementation of a single-photon-based ACI within a 10-meter drop tower, we introduce a testing concept for GR expected to substantially improve testing accuracy in atom interferometers to the level of  $10^{-5}$ . Furthermore, we anticipate that this GR testing method will derive significant benefits from space experiments, utilizing the larger velocity of atoms in interferometers located in eccentric orbits around the Earth.

#### Acknowledgements

We acknowledge instructive discussions from Yujie Tan.

#### Funding

This work was supported by the National Natural Science Foundation of China (Grant No. 11922404, 11727809, 12004128, 12104174, 12205110, and 12274613).

#### Availability of data and materials

All the data and materials relevant to this study are available from the corresponding author upon reasonable request.

#### Declarations

#### Ethics approval and consent to participate

Not Applicable.

#### Consent for publication

Not Applicable.

#### Competing interests

All authors declare that there are no competing interests.

#### Author contributions

ZH and XD conceived and instructed the research. JL and HL performed the calculation with the assistance of XD, MZ, LC, and YX. JL and YX wrote the manuscript with input from all authors. All authors read and approved the final manuscript.

Received: 2 November 2023 Revised: 20 January 2024

Accepted: 26 January 2024 Published online: 08 February 2024

#### References

1. Wagner TA, Schlamminger S, Gundlach JH, Adelberger EG (2012) Torsion-balance tests of the weak equivalence principle. *Class Quantum Gravity* 29
2. Tarallo MG, Mazzoni T, Poli N, Sutyryn DV, Zhang X, Tino GM (2014) Test of Einstein equivalence principle for 0-spin and half-integer-spin atoms: search for spin-gravity coupling effects. *Phys Rev Lett* 113
3. Williams JG, Turyshev SG, Boggs DH (2012) Lunar laser ranging tests of the equivalence principle. *Class Quantum Gravity* 29
4. Müller H, Chiow SW, Herrmann S, Chu S, Chung KY (2008) Atom-interferometry tests of the isotropy of post-Newtonian gravity. *Phys Rev Lett* 100
5. Delva P, Puchades N, Schönemann E, Dilssner F, Courde C, Bertone S, Gonzalez F, Hees A, Le Poncin-Lafitte C, Meynadier F, Prieto-Cerdeira R, Sohet B, Ventura-Traveset J, Wolf P (2018) Gravitational redshift test using eccentric Galileo satellites. *Phys Rev Lett* 121
6. Rovelli C (2005) Loop quantum gravity. In: Albert Einstein century international conference, Paris
7. Colladay D, Kostelecky VA (1997) CPT violation and the standard model. *Phys Rev D* 55:6760–6774
8. Tasson JD (2014) Gravity, CPT, and the standard-model extension. In: 5th international conference on exotic atoms and related topics (EXA). Austrian Acad Sci, Vienna
9. Herrmann S, Finke F, Lulf M, Kichakova O, Puetzfeld D, Knickmann D, List M, Rievers B, Giorgi G, Günther C, Dittus H, Prieto-Cerdeira R, Dilssner F, Gonzalez F, Schönemann E, Ventura-Traveset J, Lämmerzahl C (2018) Test of the gravitational redshift with Galileo satellites in an eccentric orbit. *Phys Rev Lett* 121
10. Takamoto M, Ushijima I, Ohmae N, Yahagi T, Kokado K, Shinkai H, Katori H (2020) Test of general relativity by a pair of transportable optical lattice clocks. *Nat Photonics* 14: 411
11. Bothwell T, Kennedy CJ, Aeppli A, Kedar D, Robinson JM, Oelker E, Staron A, Ye J (2022) Resolving the gravitational redshift across a millimetre-scale atomic sample. *Nature* 602:420
12. Zheng X, Dolde J, Cambria MC, Lim HM, Kolkowitz S (2023) A lab-based test of the gravitational redshift with a miniature clock network. *Nat Commun* 14
13. Duan XC, Deng XB, Zhou MK, Zhang K, Xu WJ, Xiong F, Xu YY, Shao CG, Luo J, Hu ZK (2016) Test of the universality of free fall with atoms in different spin orientations. *Phys Rev Lett* 117:023001
14. Zhang T, Chen LL, Shu YB, Xu WJ, Cheng Y, Luo Q, Hu ZK, Zhou MK (2023) Ultrahigh-sensitivity Bragg atom gravimeter and its application in testing Lorentz violation. *Phys Rev Appl* 20
15. Rosi G, D'Amico G, Cacciapuoti L, Sorrentino F, Prevedelli M, Zych M, Brukner C, Tino GM (2017) Quantum test of the equivalence principle for atoms in coherent superposition of internal energy states. *Nat Commun* 8:15529
16. Zhou L, Long S, Tang B, Chen X, Gao F, Peng W, Duan W, Zhong J, Xiong Z, Wang J, Zhang Y, Zhan M (2015) Test of equivalence principle at  $10^{-8}$  level by a dual-species double-diffraction Raman atom interferometer. *Phys Rev Lett* 115:013004
17. Asenbaum P, Overstreet C, Kim M, Curti J, Kasevich MA (2020) Atom-interferometric test of the equivalence principle at the  $10^{-12}$  level. *Phys Rev Lett* 125:191101
18. Zhang K, Zhou MK, Cheng Y, Chen LL, Luo Q, Xu WJ, Cao LS, Duan XC, Hu ZK (2020) Testing the universality of free fall by comparing the atoms in different hyperfine states with Bragg diffraction. *Chinese Phys Lett* 37

19. Fixler JB, Foster GT, McGuirk JM, Kasevich MA (2007) Atom interferometer measurement of the Newtonian constant of gravity. *Science* 315:74–77
20. Lamporesi G, Bertoldi A, Cacciapuoli L, Prevedelli M, Tino GM (2008) Determination of the Newtonian gravitational constant using atom interferometry. *Phys Rev Lett* 100:050801
21. Parker RH, Yu CH, Zhong WC, Estey B, Müller H (2018) Measurement of the fine-structure constant as a test of the standard model. *Science* 360: 191
22. Morel L, Yao Z, Clade P, Guellati-Khelifa S (2020) Determination of the fine-structure constant with an accuracy of 81 parts per trillion. *Nature* 588:61–65
23. Peters A, Chung KY, Chu S (2001) High-precision gravity measurements using atom interferometry. *Metrologia* 38:25–61
24. Biedermann GW, Wu X, Deslauriers L, Roy S, Mahadeswaraswamy C, Kasevich MA (2015) Testing gravity with cold-atom interferometers. *Phys Rev A* 91
25. Zhou L, Xiong ZY, Yang W, Tang B, Peng WC, Wang YB, Xu P, Wang J, Zhan MS (2011) Measurement of local gravity via a cold atom interferometer. *Chinese Phys Lett* 28
26. Hu ZK, Sun BL, Duan XC, Zhou MK, Chen LL, Zhan S, Zhang QZ, Luo J (2013) Demonstration of an ultrahigh-sensitivity atom-interferometry absolute gravimeter. *Phys Rev A* 88
27. Zhou L, Xiong ZY, Yang W, Tang B, Peng WC, Hao K, Li RB, Liu M, Wang J, Zhan MS (2011) Development of an atom gravimeter and status of the 10-meter atom interferometer for precision gravity measurement. *Gen Relativ Gravit* 43:1931–1942
28. Roura A (2020) Gravitational redshift in quantum-clock interferometry. *Phys Rev X* 10
29. Ufrecht C, Di Pumpo F, Friedrich A, Roura A, Schubert C, Schlippert D, Rasel EM, Schleich WP, Giese E (2020) Atom-interferometric test of the universality of gravitational redshift and free fall. *Phys Rev Res* 2
30. Di Pumpo F, Ufrecht C, Friedrich A, Giese E, Schleich WP, Unruh WG (2021) Gravitational redshift tests with atomic clocks and atom interferometers. *PRX Quantum* 2
31. Zych M, Brukner Č (2018) Quantum formulation of the Einstein equivalence principle. *Nat Phys* 14:1027–1031
32. Zych M, Costa F, Pikovski I, Brukner C (2011) Quantum interferometric visibility as a witness of general relativistic proper time. *Nat Commun* 2:505
33. Yao ZB, Solaro C, Carrez C, Cladé P, Guellati-Khelifa S (2022) Local phase shift due to interactions in an atom interferometer. *Phys Rev A* 106
34. Dimopoulos S, Graham PW, Hogan JM, Kasevich MA (2008) General relativistic effects in atom interferometry. *Phys Rev D* 78
35. Bordé CJ (2004) Quantum theory of atom-wave beam splitters and application to multidimensional atomic gravito-inertial sensors. *Gen Relativ Gravit* 36:475–502
36. Bordé CJ (2008) 5D optics for atomic clocks and gravito-inertial sensors. *Eur Phys J Spec Top* 163:315–332
37. Wolf P, Blanchet L, Bordé CJ, Reynaud S, Salomon C, Cohen-Tannoudji C (2011) Does an atom interferometer test the gravitational redshift at the Compton frequency? *Class Quantum Gravity* 28
38. Tan YJ, Shao CG, Hu ZK (2016) Finite-speed-of-light perturbation in atom gravimeters. *Phys Rev A* 94
39. Hu L, Poli N, Salvi L, Tino GM (2017) Atom Interferometry with the Sr optical clock transition. *Phys Rev Lett* 119
40. Roura A, Schubert C, Schlippert D, Rasel EM (2021) Measuring gravitational time dilation with delocalized quantum superpositions. *Phys Rev D* 104
41. Hu L, Wang E, Salvi L, Tinsley JN, Tino GM, Poli N (2020) Sr atom interferometry with the optical clock transition as a gravimeter and a gravity gradiometer. *Class Quantum Gravity* 37
42. Nourshargh R, Lellouch S, Hedges S, Langlois M, Bongs K, Holyński M (2021) Circulating pulse cavity enhancement as a method for extreme momentum transfer atom interferometry. *Commun Phys* 4
43. Rudolph J, Wilkason T, Nantel M, Swan H, Holland CM, Jiang YJ, Garber BE, Carman SP, Hogan JM (2020) Large momentum transfer clock atom interferometry on the 689 nm intercombination line of strontium. *Phys Rev Lett* 124
44. Chen ZL, Louie G, Wang YP, Deshpande T, Kovachy T (2023) Enhancing strontium clock atom interferometry using quantum optimal control. *Phys Rev A* 107
45. Moriya PH, Lee M, Hastie JE (2023) Low phase noise operation of a cavity-stabilized 698 nm AlGaInP-based VECSEL. *Opt Express* 31:28018–28025
46. Tino GM, Bassi A, Bianco G, Bongs K, Bouyer P, Cacciapuoli L, Capozziello S, Chen XZ, Chiofalo ML, Derevianko A, Ertmer W, Gaaloul N, Gill P, Graham PW, Hogan JM, less L, Kasevich MA, Katori H, Klempt C, Lu XH, Ma LS, Müller H, Newbury NR, Oates CW, Peters A, Poli N, Rasel EM, Rosi G, Roura A, Salomon C, Schiller S, Schleich W, Schlippert D, Schreck F, Schubert C, Sorrentino F, Sterr U, Thomsen JW, Vallone G, Vetrano F, Villoro P, von Klitzing W, Wilkowski D, Wolf P, Ye J, Yu N, Zhan MS (2019) SAGE: a proposal for a space atomic gravity explorer. *Eur Phys J D* 73
47. Canuel B, Abend S, Amaro-Seoane P, Badaracco F, Beaufils Q, Bertoldi A, Bongs K, Bouyer P, Braxmaier C, Chaibi W, Christensen N, Fitzek F, Flouris G, Gaaloul N, Gaffet S, Alzar CLG, Geiger R, Guellati-Khelifa S, Hammerer K, Harms J, Hinderer J, Holyński M, Junca J, Katsanevas S, Klempt C, Kozanitis C, Krutzik M, Landragin A, Roche IL, Leykauf B, Lien YH, Loriani S, Merlet S, Merzougui M, Nofrarias M, Papadakos P, dos Santos FP, Peters A, Plexousakis D, Prevedelli M, Rasel EM, Rogister Y, Rosat S, Roura A, Sabulsky DO, Schkolnik, Schlippert D, Schubert C, Sidorenkov L, Siemss JN, Sopaerta CF, Sorrentino F, Struckmann C, Tino GM, Tsagkatakis G, Viceré A, von Klitzing W, Woerner L, Zou X (2020) ELGAR-a European laboratory for gravitation and atom-interferometric research. *Class Quantum Gravity* 37

## Publisher's Note

Springer Nature remains neutral with regard to jurisdictional claims in published maps and institutional affiliations.

**Submit your manuscript to a SpringerOpen<sup>®</sup> journal and benefit from:**

- Convenient online submission
- Rigorous peer review
- Open access: articles freely available online
- High visibility within the field
- Retaining the copyright to your article

Submit your next manuscript at ► [springeropen.com](https://www.springeropen.com)